PHYSICAL REVIEW E **71**, 050901(R) (2005)

Pattern formation of microtubules and motors: Inelastic interaction of polar rods

Igor S. Aranson[1] and Lev S. Tsimring[2]
[1]*Argonne National Laboratory, 9700 South Cass Avenue, Argonne, Illinois, 60439, USA*
[2]*Institute for Nonlinear Science, University of California, San Diego, La Jolla, California, 92093-0402, USA*
(Received 15 June 2004; published 10 May 2005)

We derive a model describing spatiotemporal organization of an array of microtubules interacting via molecular motors. Starting from a stochastic model of inelastic polar rods with a generic anisotropic interaction kernel we obtain a set of equations for the local rods concentration and orientation. At large enough mean density of rods and concentration of motors, the model describes orientational instability. We demonstrate that the orientational instability leads to the formation of vortices and (for large density and/or kernel anisotropy) asters seen in recent experiments.

DOI: 10.1103/PhysRevE.71.050901 PACS number(s): 87.16.−b, 05.65.+b, 47.54.+r

One of the most important functions of molecular motors (MM) is to organize a network of long filaments [microtubules (MT)] during cell division to form cytoskeletons of daughter cells [1]. A number of *in vitro* experiments were performed [2–7] to study interaction of MM and MT in isolation from other biophysical processes simultaneously occurring *in vivo*. At large enough concentrations of MM and MT, the latter organize in *asters* or *vortices* depending on the type and concentration of MM.

After MM binds to a microtubule at a random position, it marches along it in a fixed direction until it unbinds without appreciable displacement of the MT. If a MM binds to *two* MTs, it can change their mutual position and orientation significantly. In Ref. [5], the interaction of rodlike filaments via motor binding and motion has been studied, and patterns resembling experimental ones were observed. In [8] a phenomenological model for the MM density and the MT orientation has been proposed. Reference [9] generalized this model by including separate densities of free and bound MM, as well as the density of the MT. They found the transition from asters to vortices, as the density of MM is increased in disagreement with experimental evidence [7] that the asters give way to vortices with *decreasing* the MM concentration. A phenomenological flux-force relation for active gels was applied in [10]. While vortex and aster solutions were obtained, an analysis of that model is difficult because of a large number of unknown parameters. In Ref. [11] a set of equations for MT density and orientation was derived by averaging conservation laws for the MT probability distribution function. However, this model does not exhibit orientation transition for homogeneous MT distributions.

Here we derive a model for the collective spatiotemporal dynamics of MTs starting with a master equation for interacting inelastic polar rods. Our model differs from the transport equations [11] in that it maintains the detailed balance of rods with a certain orientation. The model exhibits an onset of orientational order for large enough density of MT and MM, formation of vortices and then asters with increase in the MM concentration.

MMs enter the model implicitly by specifying the interaction rules between two rods. Since the diffusion of MMs is about 100 times higher than that of MTs, as the first step we neglect spatial variations of the MM density. While variable MM concentration affects certain quantitative aspects [7], our analysis captures salient features of the phenomena. All rods are assumed to be of length l and diameter $d \ll l$, and are characterized by the centers of mass $\mathbf{r}$ and orientation angle ϕ.

Maxwell model. Consider the orientational dynamics only and ignore the spatial coordinates of interacting rods [an analog of the Maxwell model of binary collisions in kinetic theory of gases (see, e.g., [12])]. Since the motor residence time on MT (about 10 s) is much smaller than the characteristic time of pattern formation (about 1 h), we model the MM-MT inelastic interaction by an instantaneous collision in which two rods change their orientations

$$\begin{pmatrix} \phi_1^a \\ \phi_2^a \end{pmatrix} = \begin{pmatrix} \gamma & 1-\gamma \\ 1-\gamma & \gamma \end{pmatrix} \begin{pmatrix} \phi_1^b \\ \phi_2^b \end{pmatrix}, \tag{1}$$

where $\phi_{1,2}^b$ are orientations before and $\phi_{1,2}^a$ after the collision, γ characterizes the inelasticity of collisions, and $|\phi_2^b - \phi_1^b| < \phi_0 < \pi$. The angle between two rods is reduced after the collision by a factor $2\gamma - 1$. $\gamma = 0$ corresponds to a totally elastic collision (the rods exchange their angles) and $\gamma = 1/2$ corresponds to a totally inelastic collision: rods acquire identical orientation $\phi_{1,2}^a = (\phi_1^b + \phi_2^b)/2$ [see Fig. 1(a)]. Here we assume that two rods only interact if the angle between them is less than ϕ_0. Because of 2π periodicity, we have to add the rule of collision between two rods with $2\pi - \phi_0 < |\phi_2^b - \phi_1^b| < 2\pi$. In this case we have to replace $\phi_1^{b,a} \to \phi_1^{b,a} + \pi$, $\phi_2^{b,a} \to \phi_2^{b,a} - \pi$ in Eq. (1). In the following we will only consider the case of totally inelastic rods ($\gamma = 1/2$) and $\phi_0 = \pi$, the generalization for arbitrary γ and ϕ_0

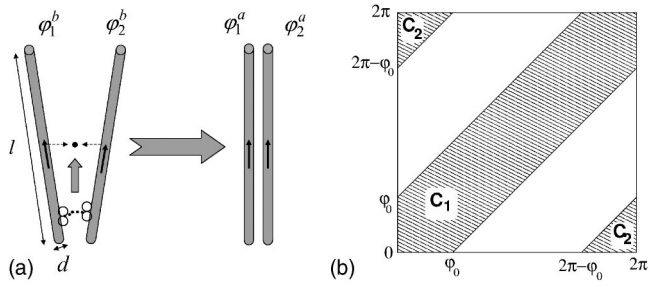

FIG. 1. (a) sketch of a motor-mediated two-rod interaction for $\gamma = 1/2$, (b) integration regions $C_{1,2}$ for Eq. (2).

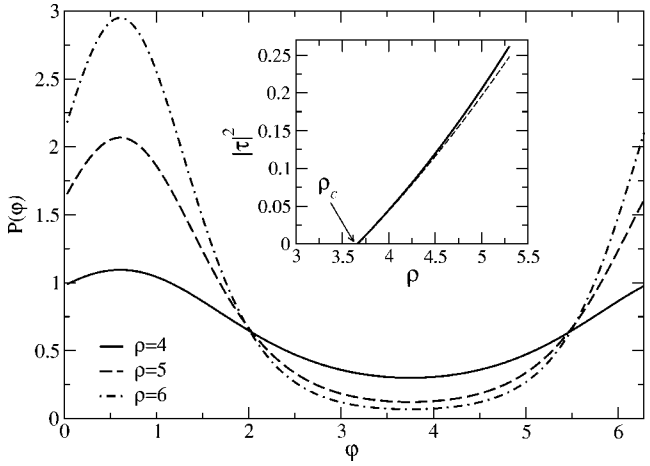

FIG. 2. Stationary solutions $P(\phi)$ for different ρ. Inset: the stationary value of $|\tau|$ vs ρ obtained from the Maxwell model (3); the dashed line is the truncated model (8).

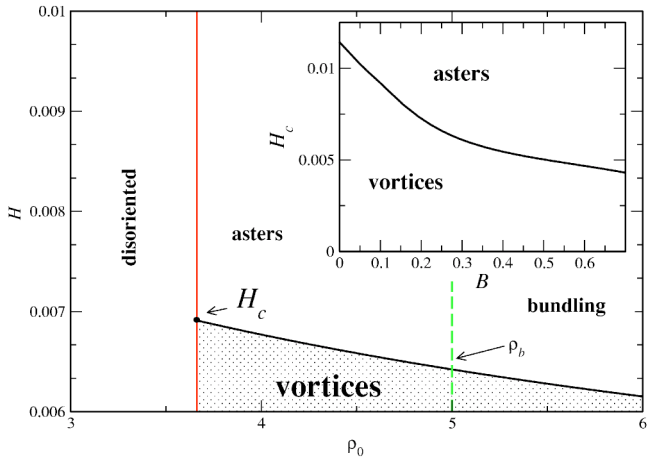

FIG. 3. Phase boundaries obtained from the linear stability analysis of aster solution for $B^2=0.05$, the dashed line shows the bundling instability limit $\rho_0>\rho_b=5$. Inset: The position of critical point H_c vs B at $\rho_0=4.5$.

is straightforward [13]. The probability $P(\phi)$ obeys the following master equation:

$$\partial_t P(\phi) = D_r \partial_\phi^2 P(\phi) + g\int_{C_1} d\phi_1 d\phi_2 P(\phi_1)P(\phi_2) \times [\delta(\phi-\phi_1/2-\phi_2/2)-\delta(\phi-\phi_2)] + g\int_{C_2} d\phi_1 d\phi_2 P(\phi_1)P(\phi_2)[\delta(\phi-\phi_1/2 - \phi_2/2-\pi)-\delta(\phi-\phi_2)], \quad (2)$$

where g is the "collision rate" proportional to the number of MM, the diffusion term $\propto D_r$ describes the thermal fluctuations of rod orientation, and the integration domains C_1, C_2 are shown in Fig. 1(b). Changing variables $t\to D_r t$, $P\to gP/D_r$, $w=\phi_2-\phi_1$, one obtains

$$\partial_t P(\phi) = \partial_\phi^2 P(\phi) + \int_{-\pi}^{\pi} dw[P(\phi+w/2)P(\phi-w/2) - P(\phi)P(\phi-w)]. \quad (3)$$

The rescaled number density $\rho=\int_0^{2\pi}P(\phi,t)d\phi$ now is proportional to the density of rods multiplied by the density of motors. Let us consider the Fourier harmonics

$$P_k = \langle e^{-ik\phi}\rangle = \frac{1}{2\pi}\int_0^{2\pi} d\phi e^{-ik\phi}P(\phi,t). \quad (4)$$

The zeroth harmonic $P_0=\rho/2\pi=$const, and the real and imaginary parts of P_1 represent the components $\tau_x=\langle\cos\phi\rangle$, $\tau_y=\langle\sin\phi\rangle$ of the average orientation vector $\boldsymbol{\tau}$, $\tau_x+i\tau_y=P_1^*$. Substituting (4) into Eq. (3) yields

$$\dot P_k + (k^2+\rho)P_k = 2\pi\sum_m P_{k-m}P_m S[\pi k/2 - m\pi]. \quad (5)$$

(here $S(x)=\sin x/x$). Due to the angular diffusion term, the magnitudes of harmonics decay exponentially with $|k|$. Assuming $P_k=0$ for $|k|>2$ one obtains from Eq. (5)

$$\dot P_1 + P_1 = 2(4-\pi)P_0P_1 - \frac{8}{3}P_2P_1^*, \quad (6)$$

$$\dot P_2 + 4P_2 = -2\pi P_0P_2 + 2\pi P_1^2. \quad (7)$$

Since near the instability threshold the decay rate of P_2 is much larger than the growth rate of P_1, we can neglect the time derivative $\dot P_2$ and obtain $P_2=AP_1^2$ with $A=2\pi(\rho+4)^{-1}$ and arrive at

$$\dot{\boldsymbol{\tau}} = \epsilon\boldsymbol{\tau} - A_0|\boldsymbol{\tau}|^2\boldsymbol{\tau}, \quad (8)$$

with $\epsilon=\rho(4\pi^{-1}-1)-1\approx 0.273\rho-1$ and $A_0=8A/3$. For large enough $\rho>\rho_c=\pi/(4-\pi)\approx 3.662$, an ordering instability leads to spontaneous rods alignment. This instability saturates at the value determined by ρ. Close to the threshold $A_0\approx 2.18$. Figure 2 shows stationary solutions $P(\phi)$ obtained from Eq. (3). As seen from the inset, the corresponding values of $|\boldsymbol{\tau}|$ are consistent with Eq. (8) up to $\rho<5.5$.

To describe the *spatial localization* of interactions, we introduce the probability distribution $P(\mathbf{r},\phi,t)$ to find a rod with orientation ϕ at location $\mathbf{r}$ at time t. The master equation for $P(\mathbf{r},\phi,t)$ can be written as

$$\partial_t P(\mathbf{r},\phi) = \partial_\phi^2 P(\mathbf{r},\phi) + \partial_i D_{ij}\partial_j P(\mathbf{r},\phi) + \int\int d\mathbf{r}_1 d\mathbf{r}_2 \int_{-\phi_0}^{\phi_0} dw\Big[W(\mathbf{r}_1,\mathbf{r}_2,\phi + w/2,\phi-w/2)P(\mathbf{r}_1,\phi+w/2)P(\mathbf{r}_2,\phi-w/2) \times\delta\left(\frac{\mathbf{r}_1+\mathbf{r}_2}{2}-\mathbf{r}\right) - W(\mathbf{r}_1,\mathbf{r}_2,\phi,\phi-w)P(\mathbf{r}_2,\phi) \times P(\mathbf{r}_1,\phi-w)\delta(\mathbf{r}_2-\mathbf{r})\Big], \quad (9)$$

where we performed the same rescaling as in Eq. (3) and dropped argument t for brevity. The first two terms in the right-hand-side of (9) describe angular and translational dif-

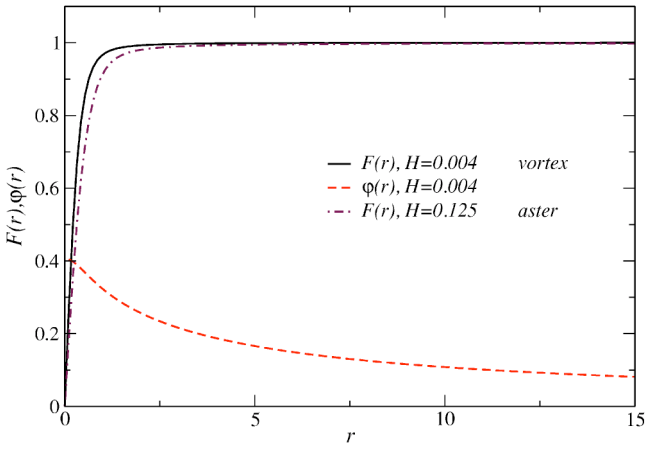

FIG. 4. Stationary vortex and aster solutions $\tau_x+i\tau_y = F(r)\exp[i\theta+i\varphi(r)]$ to Eq. (12), for $\rho_0=4$, $B^2=0.05$.

fusion of rods with the diffusion tensor $D_{ij}=(1/D_r)[D_\parallel n_i n_j + D_\perp(\delta_{ij}-n_i n_j)]$. Here $\mathbf{n}=[\cos\phi,\sin\phi]$. $D_r, D_\parallel, D_\perp$ are known in polymer physics: $D_\parallel = k_B T/\xi_\parallel$, $D_\perp = k_B T/\xi_\perp$, $D_r = 4k_B T/\xi_r$, where $\xi_\parallel, \xi_\perp, \xi_r$ are corresponding drag coefficients. For rodlike molecules, $\xi_\parallel = 2\pi\eta_s l/\log(l/d)$; $\xi_\perp = 2\xi_\parallel$; $\xi_r \approx \pi\eta_s l^3/3\log(l/d)$ where η_s is shear viscosity [14].

The last term of Eq. (9) describes the MM-mediated interaction of rods. We assume that after the interaction, the two rods acquire the same orientation and the same spatial location in the middle of their original locations. The interaction kernel W is localized in space, but in general does not have to be isotropic. On the symmetry grounds we assume the following form [we assume two-dimensional (2D) geometry and neglect higher-order anisotropic corrections]:

$$W = \frac{1}{b^2\pi}\exp\left[-\frac{(\mathbf{r}_1-\mathbf{r}_2)^2}{b^2}\right][1+\beta(\mathbf{r}_1-\mathbf{r}_2)(\mathbf{n}_1-\mathbf{n}_2)],$$

with $b \approx l = \text{const}$. This form implies that only nearby MTs interact effectively due to the MMs. The $O(\beta)$ anisotropic term describes the dependence of the coupling strength on the MT mutual orientation: "diverging" polar rods [such as shown in Fig. 1(a)] interact stronger than "converging" ones. This is the simplest term yielding nontrivial coupling between density and orientation. We perform a Fourier expansion in ϕ and truncate the series at $|n|>2$, $2\pi P_0$ gives the local number density ρ, and $P_{\pm 1}$ the local orientation $\boldsymbol{\tau}$. Omitting calculations (see [13]), rescaling space by l, and introducing parameters $B=b/l$, $H=\beta l B^2$, we arrive at

$$\partial_t\rho = \boldsymbol{\nabla}^2\left[\frac{\rho}{32}-\frac{B^2\rho^2}{16}\right]+\frac{\pi B^2 H}{16}[3\,\boldsymbol{\nabla}\cdot(\boldsymbol{\tau}\boldsymbol{\nabla}^2\rho-\rho\boldsymbol{\nabla}^2\boldsymbol{\tau}) + 2\partial_i(\partial_j\rho\partial_j\tau_i-\partial_i\rho\partial_j\tau_j)]-\frac{7\rho_0 B^4}{256}\boldsymbol{\nabla}^4\rho, \quad (10)$$

$$\partial_t\boldsymbol{\tau} = \frac{5}{192}\boldsymbol{\nabla}^2\boldsymbol{\tau}+\frac{1}{96}\boldsymbol{\nabla}(\boldsymbol{\nabla}\cdot\tau)+\epsilon\boldsymbol{\tau}-A_0|\boldsymbol{\tau}|^2\boldsymbol{\tau}+H\left[\frac{\boldsymbol{\nabla}\rho^2}{16\pi} - \left(\pi-\frac{8}{3}\right)\boldsymbol{\tau}(\boldsymbol{\nabla}\cdot\boldsymbol{\tau})-\frac{8}{3}(\boldsymbol{\tau}\boldsymbol{\nabla})\boldsymbol{\tau}\right]+\frac{B^2\rho_0}{4\pi}\boldsymbol{\nabla}^2\boldsymbol{\tau}. \quad (11)$$

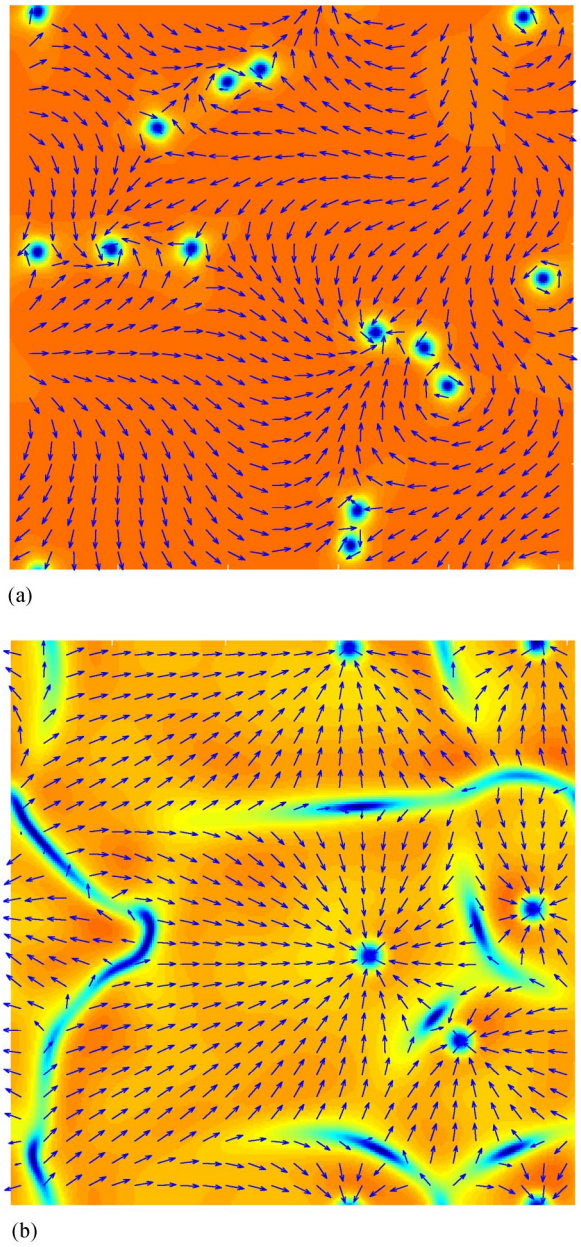

FIG. 5. Orientation τ for vortices ($H=0.006$, left) and asters ($H=0.125$, right) obtained from Eqs. (10) and (11). The color code indicates the intensity of $|\tau|$ (red corresponds to maximum and blue to zero), $B^2=0.05$, $\rho_0=4$, domain of integration 80×80 units, time of integration 1000 units.

The last two terms in Eqs. (10) and (11) are linearized near the mean density $\rho_0=\langle\rho\rangle$. The last term in Eq. (10) regularizes the short-wave instability when the diffusion term changes sign for $\rho_0>\rho_b=1/4B^2$. This instability leads to strong density variations associated with formation of MT bundles (see Fig. 3).

Aster and vortex solutions. If $B^2H \ll 1$, the density modulations are rather small, and Eq. (11) for orientation $\boldsymbol{\tau}$ decouples from Eq. (10). It is convenient to rewrite Eq. (11) for complex variable $\psi=\tau_x+i\tau_y$ in polar coordinates r,θ: $\psi=F(r)\exp[i\theta+i\varphi(r)]$ where the amplitude $F(r)$ and the phase $\varphi(r)$ are real functions. For the aster solution $\varphi(r)=0$

and for the vortex $\varphi(r) \neq 0$. Asters and vortices can be examined in the framework of a one-dimensional problem for $V=\sqrt{A_0}F(r)\exp[i\varphi(r)]$:

$$\partial_t V = D_1\Delta_r V + D_2\Delta_r V^* + (1-|V|^2)V - H\left(a_1 V \mathrm{Re}\nabla_r V + a_2\partial_r V \mathrm{Re}V + \frac{a_2 V \mathrm{Im}V}{r}\right), \quad (12)$$

where $\Delta_r=\partial_r^2+r^{-1}\partial_r-r^{-2}$, $\nabla_r=\partial_r+r^{-1}$, $D_1=1/32+\rho_0 B^2/4\pi$, $D_2=1/192$, $a_1=(\pi-8/3)/\sqrt{A_0}\approx 0.321$, $a_2=8/3\sqrt{A_0}\approx 1.81$, and we rescaled time $t\to t/\epsilon$ and space by $r\to r/\sqrt{\epsilon}$. The aster and vortex solutions for certain parameter values obtained by numerical integration of Eq. (12) are shown in Fig. 4. Vortices are observed only for small values of H and give way to asters for larger H. For $H=0$, Eq. (12) reduces to a form that was studied in [15]. It was shown in [15] that the term $\Delta_r V^*$ favors vortex solution ($\varphi=\pi/2$). In contrast, the terms proportional to H select asters. Increasing H leads to gradual reduction of φ, and at a finite $H_0(\rho_0)$ $\phi(r)=0$, i.e., the transition from vortices to asters occurs. For $0<H<H_0$, the vortex solution has a nontrivial structure. As seen in Fig. 4, the phase $\varphi\to 0$ for $r\to\infty$, i.e., vortices and asters become indistinguishable far away from the core.

The phase diagram is shown in Fig. 3. The solid line $H_0(\rho_0)$ separating vortices from asters is obtained from solution of the linearized Eq. (12) by tracking the most unstable eigenvalue λ of the aster. For this purpose the solution to Eq. (12) was sought in the form $V=F+iw\exp(\lambda t)$, where real w obeys $\hat{L}w=\lambda w$ with operator

$$\hat{L} \equiv \bar{D}\Delta_r + (1-F^2-a_1 H\nabla_r F) - a_2 H F \nabla_r \quad (13)$$

($\bar{D}=D_1-D_2$). Eq. (13) was solved by the matching-shooting method. The dashed line corresponds to the orientation transition limit $\rho_0=\rho_c$. The lines meet in a critical point $H_c=H_0(\rho_c)$ above which vortices are unstable for arbitrary small $\epsilon>0$. The phase diagram is consistent with experiments, see Ref. [5]: for low value of kernel anisotropy $H<H_c$ (possibly corresponding to kinesin motors) increase of the density ρ_0 first leads to formation of vortices and then asters. For $H>H_c$ (possibly corresponding to the second type of MM of Ref. [5]) only asters are observed.

For $H\neq 0$ well-separated vortices and asters exhibit exponentially weak interaction. For asters it follows from the fact that $\hat{L}$ is not a self-adjoint operator. Null space of $\hat{L}^\dagger$ exponentially decays at large r, $w\sim\exp[-r/L_0]$ with the screening length in the original units $L_0=\bar{D}/a_2 H\sqrt{\epsilon}$ (see [16]).

We studied Eqs. (10) and (11) numerically. Integration was performed in a two-dimensional square domain with periodic boundary conditions by a quasi-spectral method. For small H we observed vortices and for larger H asters, in agreement with the above analysis. As seen in Fig. 5, asters have unique orientation of the microtubules (here, towards the center). Asters with opposite orientation of $\boldsymbol{\tau}$ are unstable. In large domains, asters form a disordered network of cells with a cell size of the order of L_0. Neighboring cells are separated by the "shock lines" containing saddle-type defects. Starting from a random initial condition we observed initial merging and annihilation of asters. Eventually, annihilation slows down due to exponential weakening of the interaction.

We derived continuous equations for the evolution of MT concentration and orientation. We found that an initially disordered system exhibits an ordering instability similar to a nematic phase transition in ordinary polymers at high density. The important difference is that here the ordering instability is mediated by MM and can occur at arbitrary low densities of MT. At the nonlinear stage, the instability leads to experimenatlly observed formation of asters and vortices.

We thank Leo Kadanoff, Jacques Prost, and Valerii Vinokur for useful discussions. This work was supported by the U.S. DOE, Grants No. W-31-109-ENG-38 (I.A.) and DE-FG02-04ER46135 (L.T.).

[1] J. Howard, *Mechanics of Motor Proteins and the Cytoskeleton* (Springer, New York, 2000).
[2] K. Takiguchi, J. Biochem. (Tokyo) **109**, 250 (1991).
[3] R. Urrutia *et al.*, Proc. Natl. Acad. Sci. U.S.A. **88**, 6701 (1991).
[4] F. Nédélec *et al.*, Nature (London) **389**, 305 (1997).
[5] T. Surrey *et al.*, Science **292**, 1167 (2001).
[6] D. Humphrey *et al.*, Nature (London) **416**, 413 (2002).
[7] F. Nédélec, T. Surrey, and A. C. Maggs, Phys. Rev. Lett. **86**, 3192 (2001).
[8] H. Y. Lee and M. Kardar, Phys. Rev. E **64**, 056113 (2001).
[9] J. Kim *et al.*, J. Korean Phys. Soc., **42**, 162 (2003).
[10] K. Kruse *et al.*, Phys. Rev. Lett. **92**, 078101 (2004).
[11] T. B. Liverpool and M. C. Marchetti, Phys. Rev. Lett. **90**, 138102 (2003).
[12] E. Ben-Naim and P. L. Krapivsky, Phys. Rev. E **61**, R5 (2000).
[13] See EPAPS Document No. E-PLEEE8-71-R09505 for details of calculations and computer animations. A direct link to this document may be found in the online article's HTML reference section. The document may also be reached via the EPAPS homepage (http://www.aip.org/pubservs/epaps.html) or from ftp.aip.org in the directory /epaps/. See the EPAPS homepage for more information.
[14] M. Doi and S. F. Edwards, *The Theory of Polymer Dynamics* (Clarendon Press, Oxford, 1988).
[15] I. S. Aranson and L. S. Tsimring, Phys. Rev. E **67**, 021305 (2003).
[16] I. S. Aranson and L. Kramer, Rev. Mod. Phys. **74**, 99 (2002).